

1 A hydrologic feature detection algorithm to quantify  
2 seasonal components of flow regimes

3 Noelle K. Patterson<sup>1\*</sup>, Belize A. Lane<sup>2</sup>, Samuel Sandoval-Solis<sup>1</sup>, Gregory B. Pasternack<sup>1</sup>, Sarah  
4 M. Yarnell<sup>3</sup>, Yexuan Qiu<sup>1</sup>

5  
6

7 \*Corresponding author

8

- 9 1. Department of Land, Air and Water Resources, University of California, Davis  
10 2. Department of Civil and Environmental Engineering, Utah State University  
11 3. Center for Watershed Sciences, University of California, Davis

12

13

14 Cite as: Patterson, N.P., Lane, B.A., Sandoval-Solis, S., Pasternack, G.B., Yarnell, S.M., Qiu, Y.  
15 2020. A hydrologic feature detection algorithm to quantify seasonal components of flow  
16 regimes. Journal of Hydrology. DOI: 10.1016/j.jhydrol.2020.124787

17

18

19

20

21 The final version of this manuscript is available at ResearchGate at:  
22 <https://doi.org/10.1016/j.jhydrol.2020.124787>

23

## 24 Highlights

- 25 • A new signal processing algorithm identifies seasonal transitions from daily flow data.
- 26 • Application to 223 unimpaired gages in California highlights algorithm performance.
- 27 • Algorithm identifies statistically distinct seasonal timing across diverse flow regimes.

## 28 Abstract

29 Seasonal flow transitions between wet and dry conditions are a primary control on river conditions,  
30 including biogeochemical processes and aquatic life-history strategies. In regions like California with  
31 highly seasonal flow patterns and immense interannual variability, a rigorous approach is needed to  
32 accurately identify and quantify seasonal flow transitions from the annual flow regime. Drawing on  
33 signal processing theory, this study develops a transferable approach to detect the timing of seasonal  
34 flow transitions from daily streamflow time series using an iterative smoothing, feature detection, and  
35 windowing methodology. The approach is shown to accurately identify and characterize seasonal flows  
36 across highly variable natural flow regimes in California. A quantitative error assessment validated the  
37 accuracy of the approach, finding that inaccuracies in seasonal timing identification did not exceed  
38 10%, with infrequent exceptions. Results for seasonal timing were also used to highlight the  
39 statistically distinct timing found across streams with varying climatic drivers in California. The  
40 proposed approach improves understanding of spatial and temporal trends in hydrologic processes and  
41 climate conditions across complex landscapes and informs environmental water management efforts  
42 by delineating timing of seasonal flows.

## 44 Keywords

45 Streamflow hydrology, environmental flows, time series analysis, California

46

47

# 48 1. Introduction

49 Streams and rivers in semi-arid/Mediterranean climates are physically, chemically, and biologically  
50 driven by predictable, seasonal periods of wet and dry conditions over an annual cycle (Gasith and  
51 Resh 1999). Seasonal flow regimes support predictable river processes such as disturbance regimes  
52 (Rood et al. 2005), seasonal habitat provision (Aadland 1993; Booker and Acreman 2007; Jacobson  
53 2013), and native species life-history cues (Yarnell et al. 2010). While streamflow characteristics  
54 including magnitude, duration, frequency, and rate of change are useful for describing components of  
55 the flow regime (Poff et al. 1997), the timing of seasonal flow transitions within the annual flow  
56 regime is particularly important for understanding seasonally-adapted ecological processes such as  
57 migration, spawning, or vegetation recruitment (Cambray 1991; Greet et al. 2011; Poff and  
58 Zimmerman 2010). It is critical to identify these distinct wet and dry conditions and when they occur  
59 across different flow regimes to improve understanding of physical climate and watershed controls on  
60 these seasonal transitions and their sensitivity to change.

61  
62 Numerical descriptors of the flow regime, known as flow metrics, are routinely quantified from daily  
63 streamflow time series to link streamflow patterns to river processes (Buttle 2011; Poff and Ward  
64 1989) and biological response (Mazor et al. 2017; Olden and Poff 2003). Existing flow metrics used to  
65 identify and quantify the timing of seasonal flow transitions are limited, especially across large regions  
66 and in hydrologically variable settings. These measurements of timing are often simplified by  
67 calculating flow metrics within predetermined timing windows instead of identifying the occurrence of  
68 seasonal transitions and key events based on annual flow patterns. The Hydroecological Integrity  
69 Assessment Process (Henriksen et al. 2006) and the Indicators of Hydrologic Alteration (Richter et al.  
70 1996) incorporate timing through calculations such as monthly average flows or the date of annual  
71 minimum and maximum flow. However, in variable flow regimes such as flashy rain-sourced streams,  
72 the timing of seasonal flow transitions varies significantly between water years and hydroclimatic  
73 settings (Lane et al. 2018). This wide inter-annual variability suggests that metrics describing a  
74 particular aspect of seasonal flow, such as dry season flow magnitude, cannot be accurately quantified  
75 based on the same months in each water year. Calculation of the annual maximum or minimum

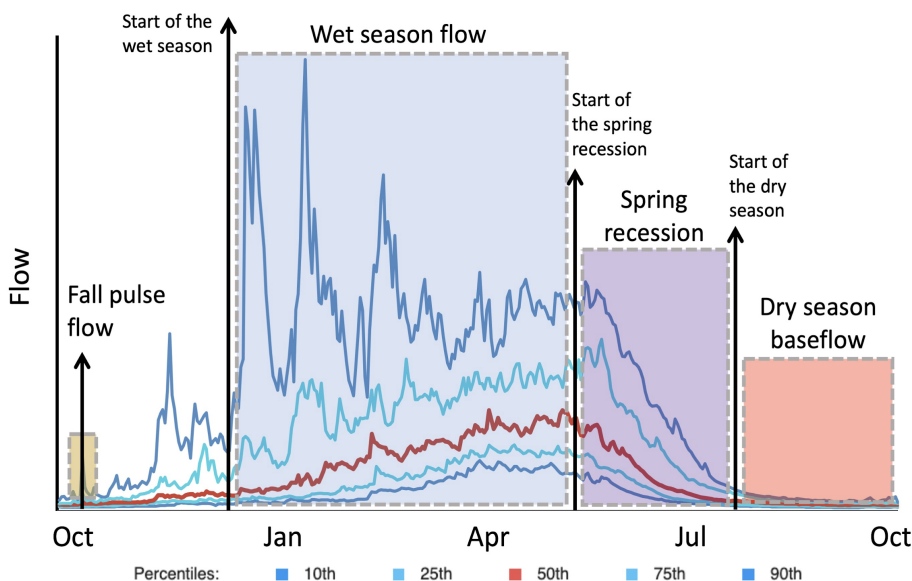
76 similarly may oversimplify understanding of seasonal flow components, because these calculations do  
77 not account for annual or seasonal patterns of flow or events other than the most extreme conditions  
78 (Déry et al. 2009).

79  
80 To better quantify flow regimes based on variable seasonal patterns, signal processing techniques can  
81 be used to identify sub-annual hydrologic patterns from daily flow time series. Signal processing  
82 theory provides well-established techniques, such as data smoothing, peak detection, and time  
83 windowing, that have been applied in hydrology (Kusche et al. 2009; Mann 2004) and can be used to  
84 detect features from a time series of daily streamflow data. Time series smoothing is used to enhance  
85 certain frequencies (i.e., the signal) while attenuating others (i.e., the noise), and many smoothing  
86 techniques are available such as moving average, exponential moving average, empirical mode  
87 decomposition, regression smoothing (e.g. LOESS, Cleaveland and Loader 1996), wavelet, and splines  
88 (Janert 2010). Smoothing functions generate fitted curves to time series data that emphasize different  
89 frequency signals depending on the function and level of smoothing (Pollock 1999). Feature detection  
90 is used to extract peaks or valleys of interest from the smoothed data and can depend on attributes  
91 such as magnitude or slope (Schneider 2011; Scholkmann et al. 2012). Dynamic windowing around a  
92 detected feature constrains further analysis to a particular period of interest and allows for increased  
93 resolution of subsequent analysis (Palshikar 2009).

94  
95 In previous work, signal processing techniques have been applied to hydrologic time series for  
96 applications such as detecting long-term trends (Letcher et al. 2001), modeling hydrologic processes  
97 (Zhang et al. 2016), and predicting future trends (Adamowski and Sun 2010; Cannas et al. 2006).  
98 Common techniques such as harmonic analysis using Fourier or wavelet transform methods can be  
99 effective in analyzing hydrologic time series characteristics, such as periodicity, trends, coherence and  
100 cross-phase among deriving and response variables, or complexity determined by wavelet entropy  
101 (Pasternack and Hinnov 2003; Sang 2013). Additionally, many techniques have been developed to  
102 identify baseflow recession (Hall 1968); recent attempts include identifying a consecutive number of  
103 days of negative slope in the hydrograph (Bart and Hope 2014), combining requirements of negative  
104 slope with a percentile-based magnitude threshold (Sawaske and Freyberg 2014), or automatic  
105 identification of recession curves based on parameters balancing accuracy and coverage (Smith and

106 Schwartz 2017). While some methods share similarities with components of the proposed method, to  
107 the authors' knowledge there has not yet been a method developed to automatically isolate and  
108 quantify all major seasonal flow transitions from annual streamflow time series.

109  
110 To identify ecologically significant flow transitions from the annual hydrograph, this study applied  
111 signal processing methods to identify functional flows found in the highly seasonal Mediterranean  
112 streams of California, USA. Functional flows refer to sub-annual aspects of the flow regime that  
113 support key ecological, geomorphic or biogeochemical processes in riverine systems (Escobar-Arias  
114 and Pasternack 2010; Yarnell et al. 2015). Yarnell et al. (2015) aggregated flow ecology literature to  
115 identify four functional flow components relevant to Mediterranean streams with a distinct wet and dry  
116 season: wet-season initiation flows, peak magnitude flows, spring recession flows, and dry-season low  
117 flows. Building on those efforts and more recent work highlighting key functional flows specific to  
118 California (Yarnell et al. 2020), this study identifies the timing of four functional flow components  
119 applicable to California's natural streamflow regimes: fall pulse flow, wet season flow (encompassing  
120 both wet season baseflow and peak flow conditions), spring recession, and dry season baseflow (Fig.  
121 1). Once the timings of functional flow transitions are identified from the annual hydrograph, each  
122 functional flow component can be further quantified using additional flow metrics such as magnitude,  
123 timing, frequency, duration, or rate of change, and can be used to design functional flow regimes in  
124 managed river systems (Yarnell et al. 2020).



125

126 Fig. 1. Identification of the start timing of four functional flows identified for California (Yarnell et al.  
127 2020) using the proposed signal processing algorithm. The timing of flow transitions identified by the  
128 algorithm are marked with arrows. Hydrographs indicate the 10<sup>th</sup>, 25<sup>th</sup>, 50<sup>th</sup>, 75<sup>th</sup>, and 90<sup>th</sup> percentiles  
129 of flow in a mixed rain-snow river system (modified from Yarnell et al. 2020). A water year in  
130 California is defined as October 1 to September 30.

131  
132 Drawing on signal processing theory, this study develops an algorithm in the open-source Python  
133 programming language to calculate the timing of seasonal flow transitions from daily flow time series,  
134 allowing for improved characterization of seasonal flows. This research addresses the following  
135 questions: (1) is it possible to automatically identify timing of seasonal streamflow components from  
136 annual hydrographs, and if so what is the level of error?; and (2) does the timing of seasonal flow  
137 components calculated through this study reveal distinctions among streams with varying climatic  
138 drivers? Using data from the highly seasonal streams of California as a testbed, this study assesses  
139 the accuracy and limitations of the algorithm for quantifying functional flows across a wide range of  
140 natural flow regimes and climate conditions, including flow regimes exhibiting snowmelt, rain, or  
141 mixed rain and snowmelt signatures. To further achieve confidence in the results, algorithm outputs  
142 are analyzed in the context of California hydrology and tested for the extent that results align with  
143 expectations for regional hydrologic regimes.

## 144 2. Methods

145 The study design describes development, calibration, and performance assessment of the algorithm  
146 for detecting the timing of functional flow transitions from daily streamflow time series, with algorithm  
147 steps summarized in Figure 4.

148

### 149 2.1. Study Region

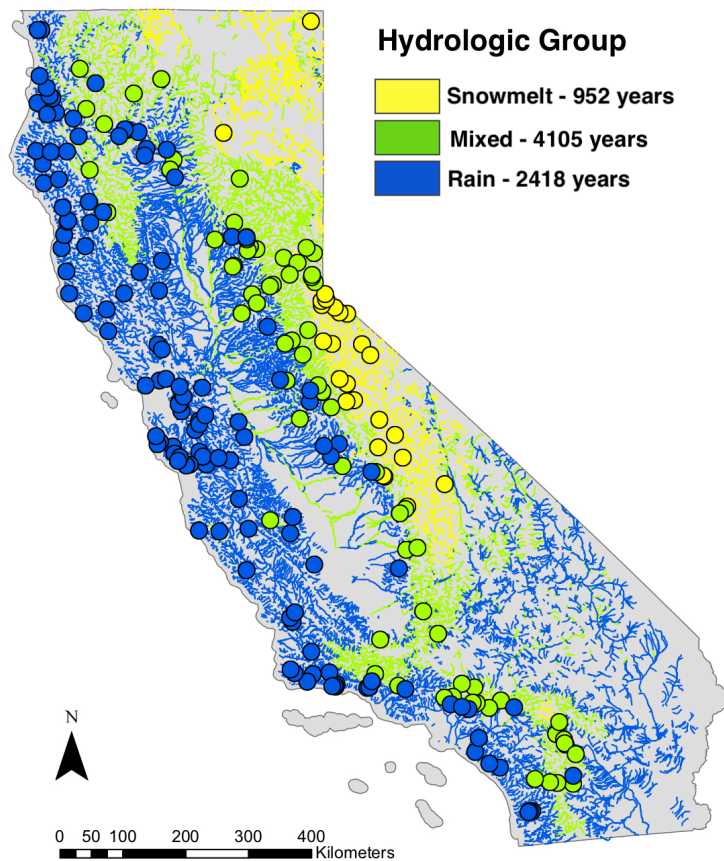
150 California has a Mediterranean climate with pronounced wet and dry seasons, as well as high  
151 interannual variability and spatial heterogeneity (Dettinger et al. 2011; Liu et al. 2018). Much of this

152 variability stems from California's wide latitudinal extent (800 km) and physiographic diversity, with  
153 multiple mountain ranges and valleys of different sizes, shapes, and relief (Abatzoglou et al. 2009;  
154 LaDochy et al. 2007). California rainfall is characterized by the capability of a limited number of high  
155 intensity storm events to contribute to the majority of annual precipitation; Dettinger et al. (2011)  
156 found that 20-50% of California's long-term rainfall average derives from these high precipitation  
157 storm events. California's rivers and streams reflect the state's climatic and physiographic diversity,  
158 ranging from small, intermittent streams in the southwest deserts to larger snowmelt-fed rivers  
159 draining the western slopes of the Sierra Nevada mountain range (Lane et al. 2018; Mount 1995).

160

161 For this study, nine natural hydrologic classes previously identified for California by Lane et al. (2018)  
162 were aggregated into three dominant stream types recognized throughout the state (Mount 1995):  
163 snowmelt-, rainfall-, and mixed snowmelt and rain-sourced streams (Fig. 2). Snowmelt-sourced flow  
164 regimes are largely controlled by the timing and rate of snowmelt, which are driven by seasonal  
165 patterns of precipitation and temperature. Rain-sourced flow regimes are controlled by the intensity of  
166 winter rainfall and characteristics of individual storm events. Mixed-source streams experience both  
167 rain-driven flows in the winter and a snowmelt pulse in the spring, or they occur in large drainages  
168 that receive both snowmelt and rainfall contributions from upstream.

Accepted Article



169

170 Fig. 2. The three dominant stream types in California based on aggregated natural hydrologic classes

171 developed by Lane et al. (2018): snowmelt (yellow), mixed snow and rain (green), and rain (blue).

172 Reference streamflow gages used in this study are shown as circles, and the number of total water

173 years of data in each stream type are shown.

## 174 2.2. Data

175 Streamflow data used for this analysis come from 223 gage stations with unimpaired or naturalized

176 daily streamflow records in California (refer to Kennard et al. 2010 for definitions of unimpaired and

177 naturalized streamflow) (Fig. 2). Unimpaired gage data was sourced from the dataset compiled by



178 Zimmerman et al. (2017), who followed a 3-step protocol to obtain unimpaired daily streamflow. Their  
179 process designated gage stations as unimpaired based on: (1) designation as a “least disturbed” site  
180 from a U.S. Geological Survey database of watershed attributes (Falcone et al. 2010), (2) status of  
181 unimpairment based on annual gage station reports and appearance of natural conditions from  
182 satellite imagery, and (3) historical flow records that pre-date anthropogenic disturbance such as  
183 dams and urbanization. Seven gages with simulated unimpaired (i.e., naturalized) daily streamflow  
184 data were also added to the dataset to cover the Central Valley region of California (CDWR 2007),  
185 which was otherwise poorly represented by unimpaired gage stations. A final screening of the annual  
186 hydrographs of the resulting dataset was performed, and several gages were removed from the  
187 analysis that had flow patterns appearing irregular, impaired, or too low to exhibit seasonal patterns.  
188 The resulting dataset of 223 reference gages includes periods of record as early as 1891 and as recent  
189 as 2015, with an average period of record of 34 years and a range of 6 to 65 years.

190

## 191 2.3. Seasonal Flow Detection Algorithm Development

192 The following sections provide the theory and rationale for the Seasonal Flow Detection Algorithm  
193 (SFDA), explain the signal processing methods applied, and describe individual calculation steps.  
194 Additional description of signal processing methods is described in the Supplemental Materials.

### 195 2.3.1. Data Smoothing

196 Data smoothing is a type of filtering in which low-frequency components are retained while high-  
197 frequency components are attenuated, enabling detection of features of interest at different  
198 frequencies or time-scales (Press and Teukolsky 1990). Common finite-difference smoothing  
199 techniques include simple running averages, weighted moving averages, and exponential filters  
200 (Janert 2010). In this study, a Gaussian weighted moving average filter was used to generate a  
201 smoothed time series using the function `gaussian_filter1d` from the SciPy Image Processing package  
202 (Verveer 2003) in Python. This smoothing method was selected for its ability to retain local maxima in

203 the output function, while avoiding abrupt distortions in the filtered data. The Gaussian filter sets the  
204 weighting factors of the smoothing window  $w_j$  according to a Gaussian normal distribution

205

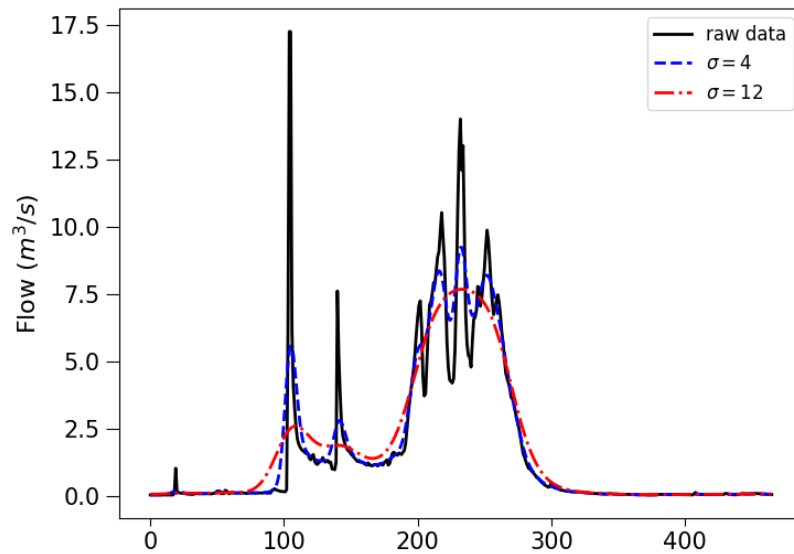
$$f(x, \sigma) = \frac{1}{\sqrt{2\pi\sigma^2}} \exp\left(-\frac{1}{2}\left(\frac{x}{\sigma}\right)^2\right) \quad [1]$$

207

208

209 such that any new streamflow observation that enters the smoothing window is only gradually added  
210 to the moving average and then gradually removed. The standard deviation of the Gaussian function  
211 ( $\sigma$ ) dictates the width of the distribution and consequently the degree of smoothing applied. In this  
212 study, low and high levels of streamflow data smoothing were associated with  $\sigma < 5$  and  $\sigma > 8$ ,  
213 respectively. For example, a daily streamflow time series smoothed with a high standard deviation  
214 Gaussian filter ( $\sigma = 12$ , Fig. 3) will dampen daily to weekly hydrologic variability while preserving major  
215 seasonal patterns. Alternatively, a low standard deviation Gaussian filter ( $\sigma = 4$ , Fig. 3) will preserve  
216 storm events occurring on weekly scales. High levels of smoothing are often applied first in the  
217 algorithm to identify coarse resolution temporal patterns such as the distinction between the annual  
218 wet and dry season, while removing the signal noise caused by individual storm events. Increasingly  
219 lower levels of smoothing are then applied to identify hydrologic features on finer temporal scales.

220



221

222 Fig. 3. Daily streamflow time series (black) plotted for one water year (Oct. 1–Sept. 30) with two  
 223 levels of filters using Gaussian weighted moving averages with different  $\sigma$  parameter values.

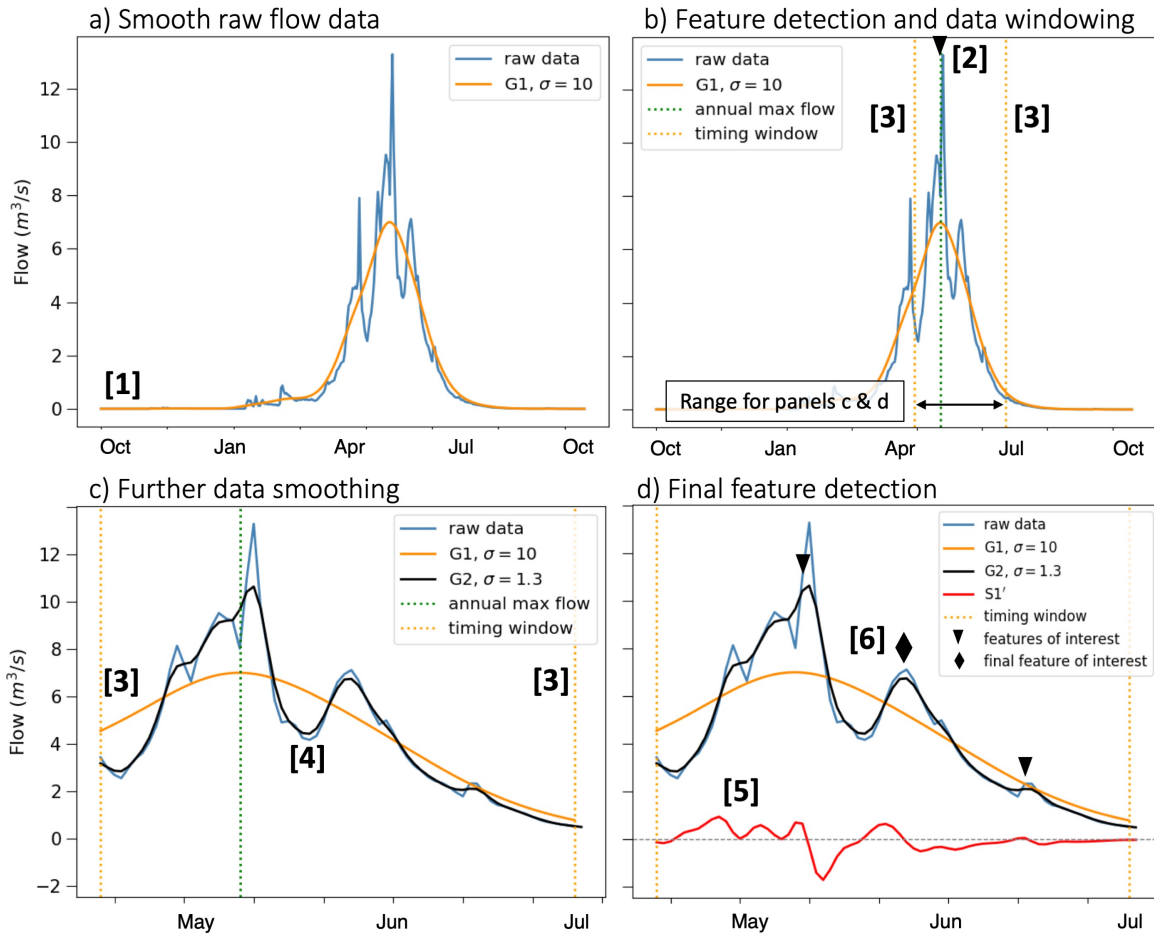
224

### 225 **2.3.2 Splines**

226 Splines are functions constructed from segments of polynomials between each time series observation  
 227 that are constrained to be smooth at the junctions (Letcher et al. 2001). Splines, which are used in  
 228 the SFDA for derivative estimation of smoothed streamflow, have been shown to generate nearly  
 229 optimal derivative estimates of noisy data such as streamflow time series due to low interpolation  
 230 error (Craven and Wahba 1978; Ragozin 1983; Thomas et al. 2015). The SFDA employs a cubic spline  
 231 function (three degrees of freedom) for derivative estimates, which is generally considered an optimal  
 232 interpolation function for large time series (Carter and Signorino, 2010; Kimball 1976; Wahba, 1978).  
 233 For further explanation on spline fitting, refer to Hastie and Tibshirani (1990). In this study, derivative  
 234 estimation using a cubic spline was performed on smoothed and windowed streamflow time series  
 235 using the one-dimensional univariate spline fitting function available from the SciPy library in Python  
 236 (Jones et al. 2001).

## 237 2.4. Seasonal Flow Detection Algorithm (SFDA) General Steps

238 The SFDA consists of six general steps used to detect seasonal flow transitions, although some  
239 applications may require either a subset of these steps or multiple iterations (Fig. 4). Steps are  
240 applied to each water year in a dataset, which in California is defined as October 1 to September 30.  
241 Step 1 (Fig. 4a): A high standard deviation Gaussian filter (G1) is applied to the observed daily  
242 streamflow time series to detect dominant peaks, valleys, or trends in the annual hydrograph.  
243 Depending on the level of smoothing, different frequency patterns (e.g., seasonal, sub-seasonal) are  
244 attenuated or left intact. Step 2 (Fig. 4b): A hydrologic feature of interest is identified from G1, such  
245 as annual peak flow. Step 3 (Fig. 4b): A localized search window is set around the feature of interest  
246 to constrain subsequent analysis to a hydrologically relevant period (e.g., 30 days before and after the  
247 feature of interest). Step 4 (Fig. 4c): Within the search window, a low standard deviation Gaussian  
248 filter (G2) is applied to the observed daily time series to extract high-resolution hydrologic patterns  
249 (e.g., individual storm events). Step 5 (Fig. 4d): A spline curve is fitted to smoothed data G2, and the  
250 derivative is taken to identify the slope of the hydrograph ( $S1'$ ). Step 6 (Fig. 4d): A feature of interest  
251 is characterized in one of two ways: i) directly from G2 using relevant flow characteristics (i.e.  
252 magnitude), or ii) using the derivative of the spline curve ( $S1'$ ) to detect peaks or valleys of interest  
253 based on slope or sign change (triangles represent peak features of interest, and the black diamond is  
254 the final selected feature).  
255



257

258 Fig. 4. Six general steps of the SFDA use data smoothing, windowing, and feature detection to identify  
 259 seasonal flow transitions from daily streamflow data.

260

261 The SFDA steps are iterative and can be repeated multiple times to consistently and accurately  
 262 identify flow transitions across water years and stream types. For example, the calculation of spring  
 263 recession requires three iterations of smoothing and feature detection, while the calculation for dry  
 264 season start timing only requires one iteration. The parameter values (e.g., smoothing parameter  $\sigma$ ,  
 265 window size, or magnitude thresholds) can be adjusted to suit the needs of particular flow regimes or  
 266 hydrologic features of interest. For example, in flashy rain-driven streams the start of the dry season  
 267 is generally indicated by the last significant storm event of the water year, which can be found using a  
 268 low standard deviation Gaussian filter that closely fits daily streamflow data. Meanwhile, the start of

269 the dry season in a snowmelt-driven stream may be better identified by the general trend of flow  
270 reduction representing catchment drainage, which is best represented with a high standard deviation  
271 Gaussian filter to capture broader trends.

272  
273 To contextualize the parameterization process, the algorithm for the dry season start timing may be  
274 considered. The dry season start timing is identified in the receding limb of the annual hydrograph  
275 through a combination of relative magnitude and slope, which are determined by parameterization.  
276 The start timing will be identified later in the water year, for example, if the relative magnitude  
277 threshold is reduced (requiring lower magnitude) or if the slope threshold is reduced (requiring a  
278 flatter slope), essentially creating more stringent hydrologic requirements. Further, the degree of  
279 smoothing applied to raw daily streamflow dampens fluctuations in flow and can allow a stabilized  
280 slope to be detected earlier in the water year as the level of smoothing is increased. The combinations  
281 of parameters for each algorithm were determined by expert opinion of the co-authors to best achieve  
282 timing of the functional flows illustrated conceptually in Figure 1 across a diversity of hydrologic  
283 inputs, and this parameterization is available as default values in the SFDA code.

284

## 285 2.5. Application of the SFDA to Functional Flows in California

286 Four distinct applications of the SFDA were used to calculate the timing of functional flow component  
287 transitions based on reference-condition California streamflow gages (Fig. 2). In these applications,  
288 the SFDA steps were repeated up to three times to accurately identify functional flow transitions  
289 across the variety of stream types found in California. The parameter values (e.g., smoothing  
290 parameter  $\sigma$  or window size) were determined heuristically by the coauthors for each functional flow  
291 component to achieve timing results aligning with the conceptual timing of functional flow transitions  
292 illustrated in Figure 1 and described in Yarnell et al. (2020). In the calibration process, parameters for  
293 each functional flow identification algorithm were empirically and incrementally adjusted to achieve  
294 hydrologically meaningful results; for example, the parameters for spring recession start timing  
295 (smoothing parameter  $\sigma$ , window sizes, and magnitude thresholds) were adjusted so that the timing  
296 would occur after wet season high flows, but before flows had receded to baseflow conditions.

297 Supplemental Materials and associated online resources provide more information about the  
298 calculation of each functional flow timing metric, how to download the SFDA code, and how to modify  
299 algorithm parameters to achieve desired results. To demonstrate SFDA application to a specific  
300 functional flow component, the calculation of wet season start timing is described in Section 2.5.1.

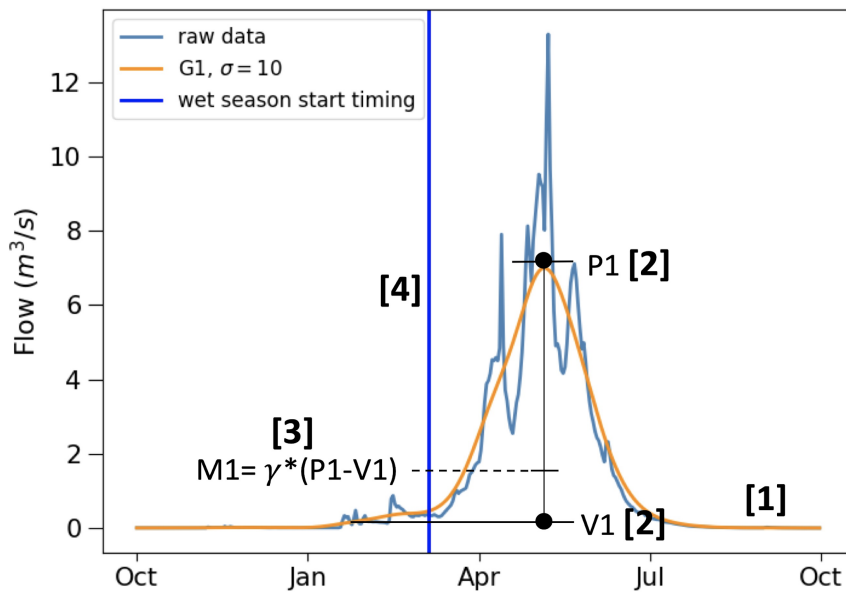
301  
302 The timing metrics from the SFDA can be used to calculate additional functional flow metrics  
303 describing the magnitude, duration, frequency, and rate of change of flow within each functional flow  
304 component (e.g., baseflow magnitude or duration of the dry season) (Yarnell et al. 2020). The full  
305 suite of SFDA-based functional flow metrics can be visualized and downloaded at [eFlows.ucdavis.edu](http://eFlows.ucdavis.edu),  
306 a website developed to view and interact with California's natural hydrology.

307

### 308 **2.5.1. Functional Flow Calculation for Wet Season Start Timing**

309 Wet season start timing delineates the portion of the water year during which streams receive the  
310 greatest inputs from storm runoff or snowmelt, and flows are elevated above dry season baseflow  
311 levels (Yarnell et al. 2020). The calculation for wet season start timing is presented as an example of  
312 the SFDA application to California functional flows. This calculation uses one iteration of the SFDA  
313 steps (Fig. 5). Within each water year, a high standard deviation Gaussian filter (G1,  $\sigma=10$ ) is applied  
314 (Fig. 5, Step 1) to detect the water year's global peak (P1) and preceding global valley (V1) (Fig. 5,  
315 Step 2). A relative magnitude threshold M1 is then set based on the magnitude of P1 and V1 as an  
316 upper limit ( $M1=\gamma*(P1-V1)$ , where  $\gamma=0.2$ ), to ensure that the wet season start timing is not set after  
317 flows have already increased during the water year (Fig. 5, Step 3). A spline curve is fit to G1 so that  
318 its derivative can be used as a hydrologic requirement in the final feature detection step. Finally,  
319 searching backwards in time from P1, the date that discharge first falls below M1 and below a rate of  
320 change equaling ( $\delta*P1$ , where  $\delta=0.002$ ) is selected as the wet season start timing (Fig. 5, Step 4).

321 The values for  $\gamma$  and  $\delta$  were adjusted for California reference streamflow based on the co-authors'  
322 expert opinions to achieve identification of the functional flows described conceptually in Figure 1 and  
323 Yarnell et al. (2020).



324  
 325 Fig. 5. SFDA steps to calculate the wet season start timing metric using data smoothing and feature  
 326 detection based on magnitude and rate of change requirements.

## 327 2.6. Performance Assessment

328 The calibrated SFDA was evaluated based on its ability to accurately determine the timing of functional  
 329 flow transitions across all years in the California unimpaired streamflow dataset. The analyzed results  
 330 consist of four flow timing metrics calculated annually for each gage (6–65 years per gage).  
 331 Performance assessment included: 1) a comparison of results across stream types, 2) visual  
 332 inspection of results, and 3) calculation of assessment indices to quantify issues in algorithm  
 333 performance.

### 335 2.6.1. Comparison of Functional Flow Timing Results across Stream Types

336 Results were grouped by stream type (rain-, snowmelt-, or mixed rain and snowmelt-sourced) and  
 337 visualized with violin plots, which use a rotated kernel density plot to depict the distribution of results.  
 338 Distinct letters above the violin plots denote groups with statistically distinct mean values based on  
 339 Tukey’s Honestly Significant Difference statistical test with a confidence level of 95% (Abdi and  
 340 Williams 2010). Groups with no statistical difference share the same letter above the violin plot.



341 Results were interpreted according to the co-authors' expert knowledge of California streamflow  
342 hydrology and supported where possible with relevant region-specific literature.

343

### 344 **2.6.2. Visual Performance Assessment**

345 Visual inspection of functional flow timing results was performed as a preliminary step to inform  
346 quantitative inspection (Section 2.6.3). The four annual flow timing metrics were reviewed for each  
347 water year in the dataset (n=7475 years), yielding 29,900 visual inspections. Accuracy was visually  
348 assessed based on the authors' knowledge of California seasonal flow components and when they  
349 were expected to occur across a range of water year types. Results that appeared incorrect were  
350 tabulated, grouped according to functional flow component and stream type, and reviewed by multiple  
351 experts in California hydrology from the co-author team to ensure consistency. After performing the  
352 29,900 visual inspections of the four timing metrics, issues were characterized based on the bias in  
353 timing (e.g., early or late timing) and the stream type in which it occurred.

354

### 355 **2.6.3. Quantitative Analysis with Assessment Indices**

356 The purpose of this analysis was to quantify issues in algorithm performance observed during visual  
357 assessment. The issues characterized during visual assessment were quantified using programmed  
358 rules defined to identify occurrence of each issue across the dataset. For example, one rule identified  
359 years in rain-sourced streams in which dry season start timing was set after August 1. This was based  
360 on repeated observation that flow magnitude and slope generally decrease to baseflow levels in this  
361 stream type before August 1, and dry season start timing set after August 1 was usually inaccurate.  
362 The developed rules were quantified across relevant stream types and resulting values were termed  
363 assessment indices. Many of the assessment indices attempt to quantify cases in which functional flow  
364 timing was either earlier or later than expected for a given water year, and these issues with timing  
365 were often stream type-specific. For example, seasonal timing metrics tend to occur later in the water  
366 year for snowmelt-sourced streams than rain-sourced streams, so a dry season timing metric of March  
367 1 could be considered anomalously early in snowmelt streams but normal in rain streams. Early or late  
368 occurrence was defined either through an empirical, evidence-based cut-off point (such as Aug. 1) or  
369 if possible through a relative hydrologic relationship, such as the number of high-flow events that  
370 occur before or after a particular timing metric is set. Other assessment indices quantify water year

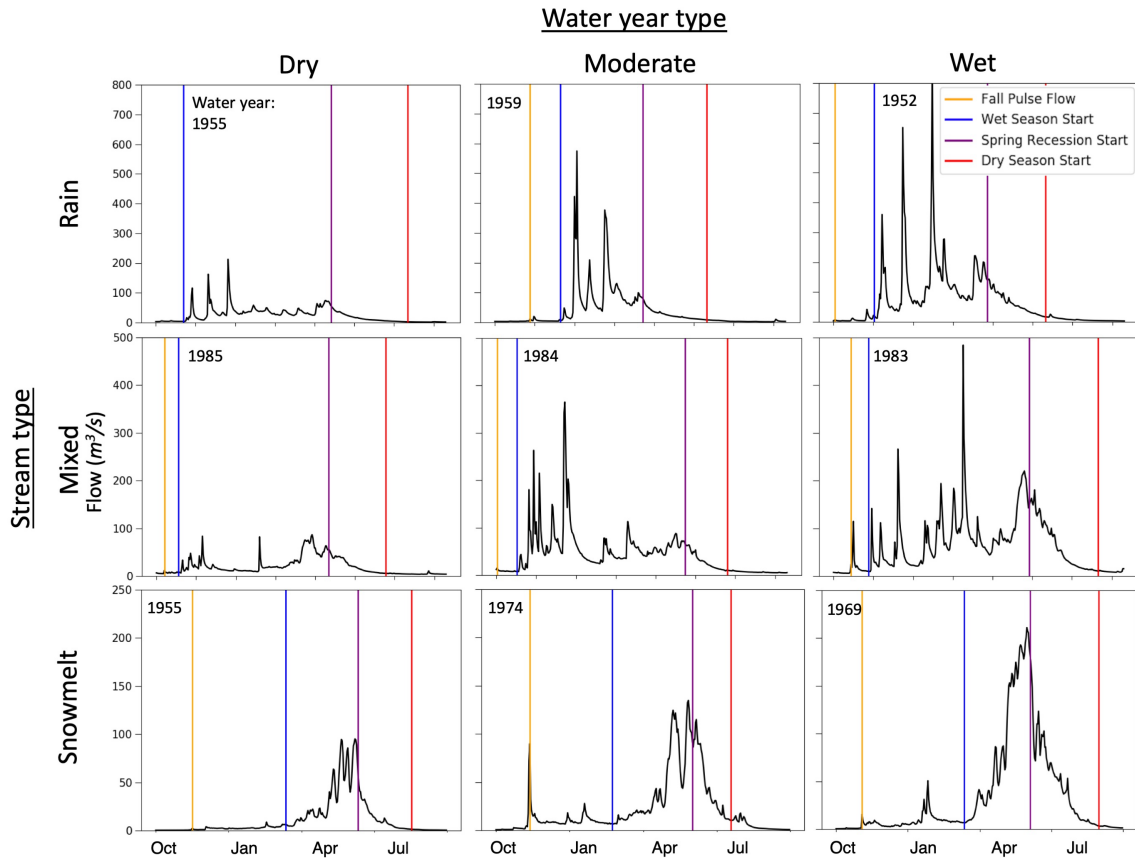
371 features that make characterization with the SFDA difficult, such as dry water years in which only one  
372 or two peak flow events occur. Table 1 lists performance assessment indices used to quantify issues in  
373 algorithm timing calculations, based on final results from the SFDA.

### 374 3. Results and Discussion

375  
376 The SFDA was found to consistently identify functional flow components across a wide range of  
377 hydrologic input data, enabling quantitative differentiation across stream types based on the timing of  
378 seasonal functional flows. Example SFDA timing results are presented in Figure 6 for individual water  
379 years spanning a range of stream types (rain-, mixed-, and snowmelt-sourced streams) and water  
380 year types (dry, moderate, and wet years) across a variety of watersheds, illustrating the ability of the  
381 SFDA to capture the timing of functional flow transitions in California across a diversity of hydrologic  
382 regimes.

383

Accepted, uncorrected



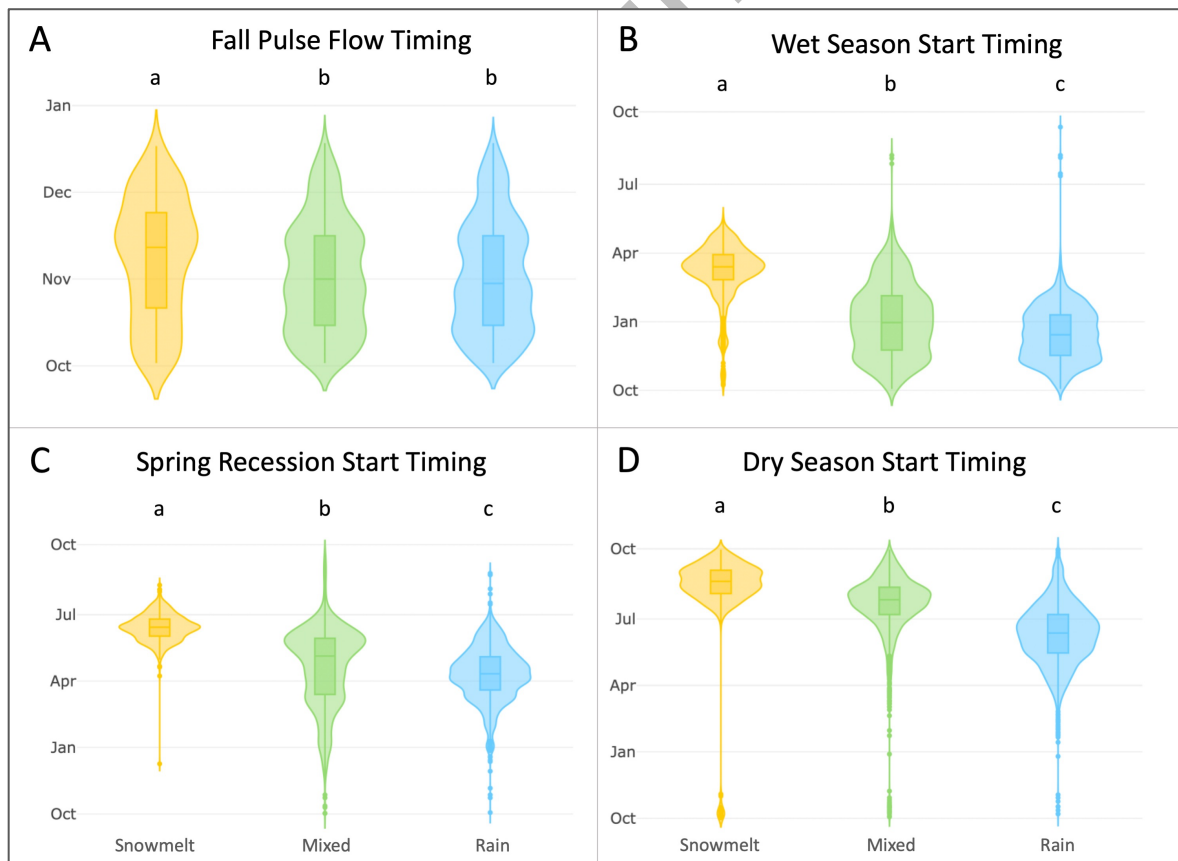
384  
 385 Fig. 6. Select SFDA results for the timing of functional flow transitions across three stream types (rain,  
 386 mixed rain and snow, and snowmelt) and three water year types in California (dry, moderate, and  
 387 wet). Individual hydrographs are from USGS gages 11529000 (rain), 11413100 (mixed rain and  
 388 snow), and 11266500 (snowmelt).

### 389 3.1. Comparison of Results across Stream Types

#### 390 3.1.1. Fall Pulse Flow Timing

391 The timing of the fall pulse flow marks the first peak flow of the water year when magnitude surpasses  
 392 baseflow in a distinct pulse. Unlike the other functional flow components, the fall pulse flow is  
 393 constrained to only occur during a subset time of the water year (Oct. 1-Dec. 15) when hydrologic  
 394 requirements for relative magnitude and duration are met, and it does not necessarily occur in each  
 395 water year. A fall pulse flow was identified in 60-65% of water years across all stream types. Although  
 396 there were significant differences in event timing ( $p < 0.05$ ) between snowmelt streams and other

397 stream types, wide overlap exists across all stream types (Fig. 7A). This is due in part to large-scale  
 398 temperature and precipitation patterns that affect California streamflow. Early in the water year (Oct.-  
 399 Nov.), temperatures across the state including the Sierra Nevada mountains are often above freezing,  
 400 causing precipitation to fall as rain or rapidly melting snow (Lundquist et al. 2008; Serreze et al.  
 401 1999). Additionally, atmospheric river events can cause correlated streamflow patterns across much of  
 402 the state (Cayan and Peterson 1989), which are most pronounced when all precipitation is falling as  
 403 rain. Therefore, a high degree of similarity is expected in the timing of fall pulse flows across all  
 404 stream types. Further reason for the limited distinction among stream classes stems from the  
 405 algorithm itself, which detects events over a narrow search window of 75 days (Oct.1-Dec. 15)  
 406 considered ecologically significant for California streams (Yarnell et al. 2015). The upper and lower  
 407 bounds of the violin plots span nearly the entire available time window of 75 days (Fig. 7A), indicating  
 408 that fall pulse flow varies widely across all stream types. These results broadly align with Ahearn et al.  
 409 (2014), who state that the season of flushing flows in California typically begins in November.  
 410



411

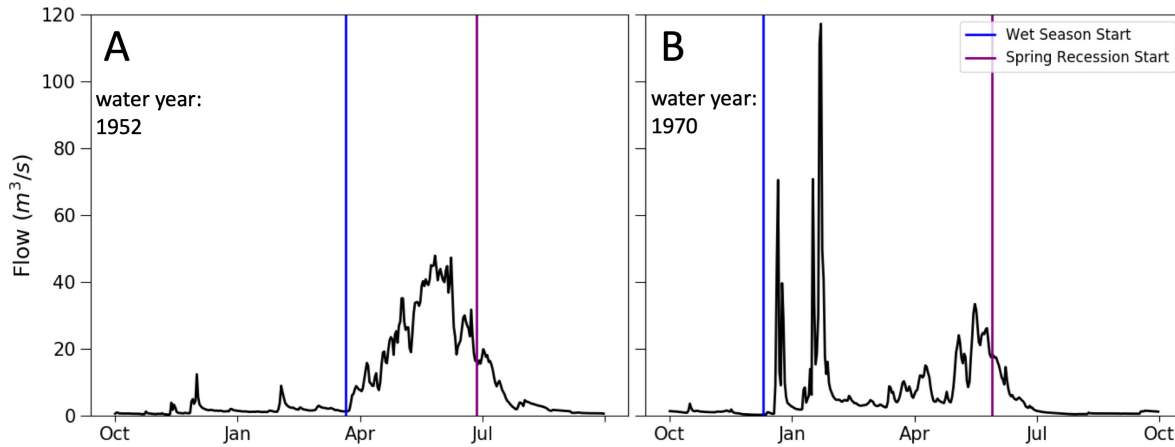
412 Fig. 7. Functional flow timing distributions across all stream types of California unimpaired streamflow.  
413 Letters above violin plots indicate statistical significance. The y-axis spans the California water year  
414 (Oct.-Sept. 31) for all components except the fall pulse flow, which is constrained from October 1-  
415 December 15.

416

### 417 **3.1.2. Wet Season Start Timing**

418 Wet season start timing is the date that the water year begins to experience consistently elevated  
419 flows from either rainfall or snowmelt (Yarnell et al. 2020). The differences in these values were  
420 statistically significant ( $p < 0.05$ ) across the three stream types (Fig. 7B). The timing occurred three to  
421 four months later in snowmelt-sourced streams (average Mar. 4) than rain-sourced streams (average  
422 Dec. 12), and timing from mixed-source streams occurred across a wide range of values whose mean  
423 (Dec. 30) closely resembles rain-sourced streams. These differences were expected due to differing  
424 geographic and climatic drivers of wet season flow across California. In rain-sourced streams, the  
425 timing of wet season flow closely reflects patterns of winter precipitation, which occurs primarily  
426 during the winter months (Dec.-Feb.), although these peak flows also experience high interannual  
427 variability in timing (Cayan and Peterson 1989; Dettinger 2011). In high elevation snowmelt-sourced  
428 streams, peak flows are initiated by the snowmelt pulse as air temperatures warm enough to melt  
429 snowpack in the spring. In mixed-source streams, wet season start timing may be cued by either  
430 winter storms or a snowmelt pulse, resulting in a wide range of possible values driven either by  
431 precipitation timing or temperature-driven snowmelt (Fig. 8). The proportion of streamflow driven by  
432 rain versus snow is an important consideration in mid- and high-elevation basins, as runoff is  
433 expected to shift towards more rain-driven flow with warming climate in the western United States

434 (Hamlet et al. 2005; Stewart et al. 2015; Sultana and Choi 2018)



435

436 Fig. 8. Hydrographs of two different water years from a mixed-source stream (USGS gage 11414000)  
437 show varying contributions of snowmelt and winter rain storms, resulting in a wide range of results for  
438 spring recession start timing and wet season start timing.

439

### 440 3.1.3. Spring Recession Start Timing

441 The spring recession represents the seasonal transition from wet season high flows to dry season low  
442 flows. The spring recession start timing is statistically distinct ( $p < 0.05$ ) across the three California  
443 stream types, with timing occurring progressively later in the water year from rain-sourced to  
444 snowmelt-sourced streams (Fig. 7C). This distinction in timing is expected due to climatic influences  
445 on hydrology that shift as streams progress from lower to higher elevations and snowpack provides  
446 increasing amounts of storage that delay streamflow response to precipitation (Aguado et al. 1992).  
447 In California's highest elevations (above 2,300 meters), the spring recession is cued by a distinct  
448 temperature-driven snowmelt pulse. As the snowmelt influence diminishes and warming occurs earlier  
449 in lower elevation mixed-source streams (Fig. 2), the snowmelt pulse may arrive earlier or may not  
450 occur at all in dry years with very little snowpack relative to rainfall. In rain-sourced streams the  
451 spring recession is expected to occur after the last rain storm of the wet season, which tends to occur  
452 several months earlier in the year than the snowmelt pulse on average. The distribution of spring  
453 recession start timings in snowmelt-sourced streams is relatively narrow, with the majority of start

454 dates occurring between May 23 and July 6 (average June 6), indicating predictable recession timing  
455 in snowmelt streams regardless of water year type (Yarnell et al. 2010).

456  
457 The most variability in spring recession start timing occurs in mixed-source streams, which due to  
458 their occurrence at mid-elevation regions are highly sensitive to changes in temperature and  
459 snowpack (Lundquist et al. 2004; Stewart 2008). Figure 8 demonstrates how a greater snowmelt  
460 pulse is associated with later spring recession timing, occurring 31 days later in water year 1952 than  
461 in 1970. This finding aligns with other research on streamflow in the western US, that has indicated  
462 both temperature and annual flow volume are significant drivers of spring snowmelt runoff timing  
463 (Aguado et al. 1992, Kormos et al. 2016). Adding to this variability, snowmelt-receiving streams in  
464 mid-elevation regions of California have been subject to significant changes in the timing of snowmelt  
465 recession peaks due to climate warming (Stewart 2008). Hamlet et al. (2005) for example estimated  
466 peak accumulation of snowmelt runoff in mid-elevation areas of California as occurring 15-45 days  
467 earlier throughout the last century, which adds additional variation to the spring recession start timing  
468 results in mixed snowmelt and rain regimes. Although rain-sourced streams also exhibit high  
469 variability in spring recession timing, the average spring recession start timing across rain-sourced  
470 streams (April 7) broadly aligns with the generally accepted end of the rainy season for California (Liu  
471 et al. 2018).

472

#### 473 **3.1.4. Dry Season Baseflow Start Timing**

474 The start timing of the dry season marks the beginning of the low flow, low variability portion of the  
475 water year, in which the rate of recession flows has stabilized and magnitudes reach baseflow level.  
476 Similar to spring recession start timing, dry season start timing is statistically distinct among the three  
477 stream types ( $p < 0.05$ ) and occurs gradually later on average from rain-sourced (June 6), to mixed-  
478 source (July 16), to snowmelt-sourced streams (August 7) (Fig. 7D). The timing distribution ranges  
479 more than 100 days in rain-sourced streams, which is consistent with the high inter-annual variability  
480 of precipitation magnitude and timing (and consequently streamflow) exhibited in California (Dettinger  
481 et al. 2011).

482

483 Despite high variability across rain-sourced streams, the average dry season start timing in these  
 484 streams is surprisingly consistent from small to large streams. For instance, the average dry season  
 485 start timing is June 8 in larger north coast streams (average annual flow 23 cms), and is similar in  
 486 flashy ephemeral streams (average annual flow 0.5 cms), with an average start timing of May 27  
 487 (from Lane et al. 2017). However, interannual variability in dry season start timing within a single  
 488 stream can be high, suggesting that central tendencies do not represent dry season timing conditions  
 489 well in rain-sourced streams.

### 490 3.2. Performance Assessment Indices

491 Assessment indices were created to quantify the accuracy of the SFDA for identifying the timing of  
 492 functional flow transitions in California reference streamflow. Assessment indices are presented in  
 493 Table 1, and the following section highlights key issues and limitations for each functional flow. The  
 494 frequency of most identified issues was less than 10%, except for Snow-early-wet and Mixed-early-  
 495 spring, which are explained in Table 1 and below.

496  
 497 Table 1. Assessment indices for SFDA timing results.

Stream type	Issue	Assessment index calculation	Index name	Frequency
All types	Fall pulse flow timing can occur on the very first day of the water year (Oct. 1), when it is difficult to determine from an annual hydrograph if the set date represents an actual peak or if it is capturing a recessing flow carried over from the previous water year.	Percentage of years in which the fall pulse timing is on day one of the water year (Oct. 1).	Fall-day1	1%
All types	Occasionally the requirements for wet season start timing are not met so the metrics are not calculated.	Percentage of years in which spring recession or dry season start timing are calculated, but wet season start timing is not	Wet-season	2%



		calculated.		
All types	A lag between spring recession and dry season start timing of more than five months indicates an anomaly within the water year, such as early spring recession or late dry season start timing, or a year in which the component timings were based off of a very limited number of storms.	Percentage of years in which the number of days between spring recession and dry season start timing is greater than 150 days (five months).	Spring-dry-gap	5%
Snowmelt	Spring recession start timing can be calculated late into the recession period such that it occurs at the end of the snowmelt pulse instead of the beginning. Dry season start timing consequently occurs very soon after the spring recession timing.	Percentage of years in which spring recession start timing and dry season start timing occur within 21 days of each other.	Snow-late-spring	1%
Snowmelt	Wet season start timing in snowmelt streams can be triggered by large rainstorm flows early in the climatic wet season (Nov.-Jan.), and other years it is triggered by the snowmelt pulse (Apr.-May). This results in a wide range of start timing in the snowmelt stream type, triggered by differing hydrologic cues. Identification of timing before February 1 approximates how often wet season start timing is triggered by rainstorms instead of snowmelt.	Percentage of years in which wet season start timing occurs before February 1.	Snow-early-wet	25%
Mixed-source and Rain	In especially dry years, the annual hydrograph can be defined by a single large, brief storm event. This may cause wet season and spring recession start timing to be set based on a single storm such that they occur in close proximity.	Percentage of years in which wet season and spring recession start timing occur within 30 days of each other.	Mixed-spring-wet/Rain-spring-wet	Mixed-spring-wet: 4%/ Rain-spring-wet: 4%

Mixed-source and Rain	Spring recession start timing can occur before the end of wet season occurrence. This most commonly occurs in hydrographs without a strong snowmelt presence.	Percentage of years in which any high flows (>5 <sup>th</sup> percentile) occur after that year's spring recession start date.	Mixed-early-spring/Rain-early-spring	Mixed-early-spring: 21%/ Rain-early-spring: 5%
Mixed-source	Dry season start timing can occur immediately after spring recession start timing, with a small gap of time between. This often occurs when the spring recession is identified too late into the period of receding high flows.	Percentage of years in which spring recession and dry season start timing occur within 21 days of each other.	Mixed-late-spring	1%
Rain	Wet season start timing can occur late after the first high flows of the wet season.	Percentage of years in which any high flows (>5 <sup>th</sup> percentile) occur before that year's wet season start date.	Rain-late-wet	8%
Rain	Dry season start timing can occur late into the dry season in rain-sourced streams, well after flows have already receded. This is usually the case when dry season start timing is set in August or later, based on repeated visual inspection.	Percentage of years in which dry season start timing occurs later than August 1.	Rain-late-dry	10%

498

499 The methods presented here to identify hydrologic features and determine error differ from previous  
500 hydrologic studies, which can often take advantage of validated training sets to determine accuracy  
501 (Cannas et al. 2006; Letcher et al. 2001; Smith and Schwartz 2017). The heuristic methods used in  
502 this research are similar to other approaches that require some subjectivity for parameterization of  
503 peak detection (Palshikar 2009), and qualitative visual assessment methods are similar to approaches  
504 used to validate climate patterns in climate modeling studies that pair qualitative and quantitative  
505 model assessment (Gyalistras et al. 1994; Paul and Hsu 2012). Performance assessment based on  
506 validation of known hydrologic conditions employed in this study is similar to the approach of Déry et

507 al. (2009), who assessed a new method of spring recession identification across different river types in  
508 their study region. The proposed methods, although subjective in the choice of parametrization,  
509 present a consistent and repeatable way to identify functional flow components, advancing previous  
510 methods of quantifying seasonal streamflow patterns.

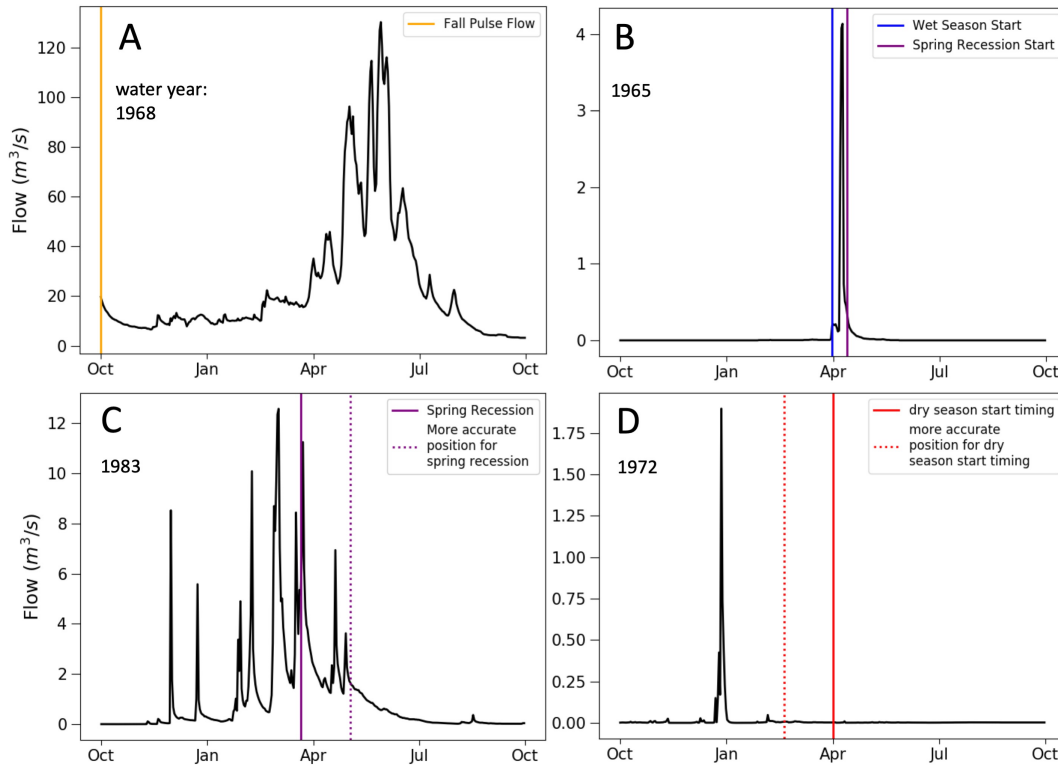
511

### 512 3.2.1. Issues in SFDA performance

513 Figure 9 presents common issues in the SFDA for each functional flow component, which were often  
514 attributed to uncommon hydrologic patterns or effects from smoothing filters that occasionally have  
515 the undesired effect of over-dampening storm peaks while detecting broad hydrologic trends. In some  
516 water years, the first day of the water year (Oct.1) was identified as the date of the fall pulse flow,  
517 which presents ambiguity as to whether the first day of the water year is an actual peak event or is  
518 instead part of a continual decline from a peak in the previous water year (Fig. 9A). This situation  
519 occurs most often in naturalized gage data, with a 3.5% occurrence rate across all naturalized water  
520 years and an average occurrence rate of 1% across the entire dataset (Table 1, index WSI-day1).

521

Accepted, uncorrected



522

523 Fig. 9. Examples in which timing metrics are affected by uncommon hydrologic patterns (A and B) or  
 524 are identified earlier or later than expected given expert understanding (C and D). Panels C and D  
 525 illustrate the algorithm results compared to proposed improvements based on the co-authors'  
 526 understanding of California hydrology. Hydrographs from USGS gages 11213500 (A), 11046300 (B),  
 527 11033000 (C), and 11120520 (D).

528

529 Both mixed- and rain-sourced streams experienced some water years in which a single large high flow  
 530 event dominated the annual hydrograph such that start timings of wet season and spring recession  
 531 were based on the same peak flow (Fig. 9B). This occurred in 4% of mixed-source streams and 4% of  
 532 rain-sourced streams (Table 1, indices Mixed-spring-wet/Rain-spring-wet) and could result in  
 533 anomalous functional flow metrics based on these rare hydrologic conditions. In mixed-source  
 534 streams, early identification of spring recession start timing was found with a frequency of 21% (Table  
 535 1, index Mixed-early-spring), sometimes due to the effect of over-dampening rainstorm peaks with  
 536 smoothing filters when attempting to detect broad hydrologic trends (Fig. 9C). Conversely, spring  
 537 recession start timing occurred late in 10% of snowmelt stream water years, when the algorithm was

538 triggered by small peaks along the recession limb instead of the main snowmelt pulse (Table 1, index  
539 Snow-early-spring). The algorithm for dry season start timing assesses the change in magnitude and  
540 slope along the recession limb, so dry water years with very little change in these features are more  
541 likely to have issues with component detection. This was often the case when dry season start timing  
542 was identified late in the water year (Fig. 9D), which occurred in 10% of rain-sourced water years  
543 (Table 1, index Rain-late-dry). These issues are expected to improve when SFDA parameters are  
544 calibrated for smaller regions of streamflow data, instead of applying the same set of parameters  
545 across a wide array of input data, as was done in this statewide case study.

## 546 4. Conclusions

547 This study developed an objective signal processing algorithm to address the need for a robust  
548 method to characterize the timing of seasonal flow transitions from daily streamflow time series. The  
549 Seasonal Flow Detection Algorithm (SFDA) improved on existing methods that rely on fixed time steps  
550 through the novel application of established signal processing techniques to identify the timing of  
551 seasonal flow transitions. The application to California streams demonstrated the ability of this  
552 approach to identify the timing of functional flow components from unimpaired daily streamflow time  
553 series across a wide range of climatic and geographic settings and extreme seasonal and interannual  
554 hydrologic variability. Results highlight hydrologic distinctions among varying drivers of streamflow,  
555 such as progressively later timing of spring recession flow as streams shift from rainfall-sourced to  
556 snowmelt-sourced flow regimes. Limitations of the approach were determined through a combination  
557 of visual expert-based assessment and quantitative performance assessment. In general, the  
558 percentage error in timing calculations did not exceed 10% across relevant water years for any  
559 assessment index, with infrequent exceptions. In a parallel effort, functional flow metrics produced by  
560 the SFDA for California reference gages are being extrapolated to ungaged streams to inform  
561 statewide environmental flow recommendations. Likewise, the SFDA has potential to be applied to  
562 other regions or countries sharing highly seasonal climates similar to California, by adjusting algorithm  
563 parameters to suit local hydrology. For instance, the SFDA metrics could be applied to assess shifts in  
564 streamflow due to climate change, with particular focus on potential changes in timing of seasonal

565 flows. The proposed approach supports improved understanding of high-resolution spatial and  
566 temporal trends in hydrologic processes and climate conditions across complex landscapes and can  
567 inform environmental water management efforts.

## 568 Acknowledgements

569 This work was supported by the UC Davis Hydrologic Sciences Graduate Group; the California State  
570 Water Resources Control Board [Grant number 16-062-300]; Utah Water Research Laboratory; and  
571 funding for G.B. Pasternack was provided by the USDA National Institute of Food and Agriculture  
572 [Hatch project number # CA-DLAW- 7034-H]. We thank Jason Hwan and two anonymous reviewers  
573 for improving the manuscript with insightful comments.

## 574 References

- 575 Aadland, L. (1993). Stream Habitat Types: Their Fish Assemblages and Relationship to Flow. *North*  
576 *American Journal of Fisheries Management*, 13(4), 790–806. [https://doi.org/10.1577/1548-](https://doi.org/10.1577/1548-8675(1993)013<0790:shtfa>2.3.co;2)  
577 [8675\(1993\)013<0790:shtfa>2.3.co;2](https://doi.org/10.1577/1548-8675(1993)013<0790:shtfa>2.3.co;2)
- 578 Abatzoglou, J. T., Redmond, K. T., & Edwards, L. M. (2009). Classification of Regional Climate  
579 Variability in the State of California. *Journal of Applied Meteorology and Climatology*, 48,  
580 1527–1541. <https://doi.org/10.1175/2009JAMC2062.1>
- 581 Abdi, H., & Williams, L. J. (2010). Tukey' s Honestly Significant Difference (HSD) Test. In  
582 *Encyclopedia of Research Design* (pp. 1–5). Thousand Oaks, CA: Sage.
- 583 Adamowski, J., & Sun, K. (2010). Development of a coupled wavelet transform and neural network  
584 method for flow forecasting of non-perennial rivers in semi-arid watersheds. *Journal of*  
585 *Hydrology*, 390(1–2), 85–91. <https://doi.org/10.1016/j.jhydrol.2010.06.033>
- 586 Aguado, E., Cayan, D., Riddle, L., & Roos, M. (1992). Climatic Fluctuations and the Timing of West  
587 Coast Streamflow. *Journal of Climate*, 5, 1468–1483.

588 Ahearn, D. S., Sheibley, R. W., Dahlgren, R. A., & Keller, K. E. (2004). Temporal dynamics of  
589 stream water chemistry in the last free-flowing river draining the western Sierra Nevada,  
590 California. *Journal of Hydrology*, 295(1–4), 47–63. <https://doi.org/10.1016/j.jhydrol.2004.02.016>

591 Bart, R., & Hope, A. (2014). Inter-seasonal variability in baseflow recession rates: The role of aquifer  
592 antecedent storage in central California watersheds. *Journal of Hydrology*, 519, 205–213.  
593 <https://doi.org/10.1016/j.jhydrol.2014.07.020>

594 Booker, D. J., & Acreman, M. C. (2007). Generalisation of physical habitat-discharge relationships.  
595 *Hydrology and Earth System Sciences*, 11(1), 141–157.

596 Buttle, J. M. (2011). Streamflow response to headwater reforestation in the Ganaraska River basin,  
597 southern Ontario, Canada. *Hydrological Processes*, 25, 3030–3041.  
598 <https://doi.org/10.1002/hyp.8061>

599 Cambray, J. A. (1991). The effects on fish spawning and management implications of impoundment  
600 water releases in an intermittent South African river. *Regulated Rivers: Research &  
601 Management*, 6(1), 39–52. <https://doi.org/10.1016/j.etc.2010.04.018>

602 Cannas, B., Fanni, A., See, L., & Sias, G. (2006). Data preprocessing for river flow forecasting using  
603 neural networks: Wavelet transforms and data partitioning. *Physics and Chemistry of the  
604 Earth*, 31(18), 1164–1171. <https://doi.org/10.1016/j.pce.2006.03.020>

605 Carter, D. B., & Signorino, C. S. (2010). Back to the Future : Modeling Time Dependence in Binary  
606 Data. *Political Analysis*, 18, 271–292. <https://doi.org/10.1093/pan/mpq013>

607 Cayan, D. R., & Peterson, D. H. (1989). The Influence of North Pacific Atmospheric Circulation on  
608 Streamflow in the West. *Geophysical Monograph*, 55, 375–397.

609 CDWR (California Department of Water Resources), 2007. *California Central Valley Unimpaired  
610 Flow Data*. (2007). Bay-Delta Office; California Department of Water Resources. Sacramento;  
611 California. [http://www.waterboards.ca.gov/waterrights/water\\_iss  
612 grams/bay\\_delta/bay\\_delta\\_plan/water\\_quality\\_control\\_plan](http://www.waterboards.ca.gov/waterrights/water_issues/programs/bay_delta/bay_delta_plan/water_quality_control_plan)

613 Cleaveland, W. S., & Loader, C. (1996). Smoothing by Local Regression: Principles and Methods. In  
614 *Statistical theory and computational aspects of smoothing* (pp. 10–49). Physica-Verlag HD.  
615 <https://doi.org/10.2307/1271204>

616 Craven, P., & Wahba, G. (1979). Smoothing noisy data with spline functions - Estimating the correct  
617 degree of smoothing by the method of generalized cross-validation. *Numerische Mathematik*,  
618 *31*(4), 377–403. <https://doi.org/10.1007/BF01404567>

619 Dettinger, M. (2011). Climate change, atmospheric rivers, and floods in California - a multimodel  
620 analysis of storm frequency and magnitude changes. *Journal of the American Water*  
621 *Resources Association*, *47*(3), 514–523. <https://doi.org/10.1111/j.1752-1688.2011.00546.x>

622 Dettinger, M. D., Ralph, F. M., Das, T., Neiman, P. J., & Cayan, D. R. (2011). Atmospheric Rivers,  
623 Floods and the Water Resources of California. *Water*, *3*(4), 445–478.  
624 <https://doi.org/10.3390/w3020445>

625 Déry, S. J., Stahl, K., Moore, R. D., Whitfield, P. H., Menounos, B., & Burford, J. E. (2009).  
626 Detection of runoff timing changes in pluvial, nival, and glacial rivers of western Canada. *Water*  
627 *Resources Research*, *45*, 1–11. <https://doi.org/10.1029/2008WR006975>

628 Escobar-Arias, M. I., & Pasternack, G. B. (2010). A hydrogeomorphic dynamics approach to assess  
629 in-stream ecological functionality using the functional flows model, part 1—model  
630 characteristics. *River Research and Applications*, *26*(9), 1103–1128.  
631 <https://doi.org/10.1002/rra.1316>

632 Falcone, J. A., Carlisle, D. M., Wolock, D. M., & Meador, M. R. (2010). GAGES : A stream gage  
633 database for evaluating natural and altered flow conditions in the conterminous United States.  
634 *Ecology*, *91*(2), 621.

635 Gasith, A., & Resh, V. H. (1999). Streams in Mediterranean Climate Regions: Abiotic Influences and  
636 Biotic Responses to Predictable Seasonal Events. *Annual Review of Ecology and Systematics*,  
637 *30*, 51–81. <https://doi.org/10.1146/annurev.ecolsys.30.1.51>



638 Greet, J., Webb, J. A., & Cousens, R. D. (2011). The importance of seasonal flow timing for riparian  
639 vegetation dynamics: a systematic review using causal criteria analysis. *Freshwater Biology*,  
640 56, 1231–1247. <https://doi.org/10.1111/j.1365-2427.2011.02564.x>

641 Gyalistras, D., Storch, H. Von, Fischlin, A., & Beniston, M. (1994). Linking GCM-simulated climatic  
642 changes to ecosystem models: case studies of statistical downscaling in the Alps. *Climate*  
643 *Research*, 4, 167–189.

644 Hall, F. R. (1968). Base-Flow Recessions—A Review. *Water Resources Research*, 4(5), 973–983.  
645 <https://doi.org/10.1029/WR004i005p00973>

646 Hamlet, A. F., Mote, P. W., Clark, M. P., & Lettenmaier, D. P. (2005). Effects of temperature and  
647 precipitation variability on snowpack trends in the Western United States. *Journal of Climate*,  
648 18(21), 4545–4561. <https://doi.org/10.1175/JCLI3538.1>

649 Hastie, T. J., & Tibshirani, R. (1990). *Generalized Additive Models*. Chapman and Hall.

650 Henriksen, B. J. A., Heasley, J., Kennen, J. G., & Nieswand, S. (2006). *Users' Manual for the*  
651 *Hydroecological Integrity Assessment Process Software (including the New Jersey*  
652 *Assessment Tools)*.

653 Jacobson, R. B. (2013). Riverine Habitat Dynamics. In J. J. Shroder, D. Butler, & C. Hupp (Eds.),  
654 *Treatise on Geomorphology* (pp. 6–19). San Diego, CA: Academic Press.  
655 <https://doi.org/10.1016/B978-0-12-374739-6.00318-3>

656 Janert, P. K. (2010). *Data Analysis with Open Source Tools* (1st ed.). O'Reilly Media, Inc.

657 Jones, E., Oliphant, T., & Peterson, P. (2001). SciPy: Open source scientific tools for Python.  
658 Online; accessed 2017-09-21. Retrieved from <http://www.scipy.org/>

659 Kennard, M. J., Mackay, S. J., Pusey, B. J., Olden, J. D., & Nick, M. (2010). Quantifying Uncertainty  
660 in Estimation of Hydrologic Metrics for Ecohydrological Studies. *River Research and*  
661 *Applications*, 26, 137–156. <https://doi.org/10.1002/rra.1249>

662 Kimball, B. A. (1976). Smoothing Data with Cubic Splines. *Agronomy Journal*, 68, 126–129.

663 Kormos, P. R., Luce, C. H., Wegner, S. J., & Berghuijs, W. R. (2016). Trends and sensitivities of low  
664 streamflow extremes to discharge timing and magnitude in Pacific Northwest mountain  
665 streams. *Water Resources Research*, 52, 4990–5007. <https://doi.org/10.1002/2015WR018125>.

666 Kusche, J., Schmidt, R., Petrovic, S., & Rietbroek, R. (2009). Decorrelated GRACE time-variable  
667 gravity solutions by GFZ, and their validation using a hydrological model. *Journal of Geodesy*,  
668 83, 903–913. <https://doi.org/10.1007/s00190-009-0308-3>

669 LaDochy, S., Medina, R., & Patzert, W. (2007). Recent California climate variability: spatial and  
670 temporal patterns in temperature trends. *Climate Research*, 33, 159–169.

671 Lane, B. A., Dahlke, H. E., Pasternack, G. B., & Sandoval-Solis, S. (2017). Revealing the Diversity  
672 of Natural Hydrologic Regimes in California with Relevance for Environmental Flows  
673 Applications. *Journal of the American Water Resources Association*, 53(2), 411–430.  
674 <https://doi.org/10.1111/1752-1688.12504>

675 Lane, B. A., Sandoval-solis, S., Stein, E. D., Yarnell, S. M., Pasternack, G. B., & Dahlke, H. E.  
676 (2018). Beyond metrics? The role of hydrologic baseline archetypes in environmental water  
677 management. *Environmental Management*, 62(4), 678–693. [https://doi.org/10.1007/s00267-](https://doi.org/10.1007/s00267-018-1077-7)  
678 [018-1077-7](https://doi.org/10.1007/s00267-018-1077-7)

679 Letcher, R. A., Yu Schreider, S., Jakeman, A. J., Neal, B. P., & Nathan, R. J. (2001). Methods for  
680 the analysis of trends in streamflow response due to changes in catchment condition.  
681 *Environmetrics*, 12(7), 613–630. <https://doi.org/10.1002/env.486>

682 Liu, Y. C., Di, P., Chen, S. H., & DaMassa, J. (2018). Relationships of rainy season precipitation and  
683 temperature to climate indices in California: Long-Term variability and extreme events. *Journal*  
684 *of Climate*, 31(5), 1921–1942. <https://doi.org/10.1175/JCLI-D-17-0376.1>

685 Lundquist, J. D., Cayan, D. R., & Dettinger, M. D. (2004). Spring Onset in the Sierra Nevada: When  
686 Is Snowmelt Independent of Elevation? *Journal of Hydrometeorology*, 5, 327–342.

687 Lundquist, J. D., Neiman, P. J., Martner, B., White, A. B., Gottas, D. J., & Ralph, F. M. (2008). Rain  
688 versus Snow in the Sierra Nevada, California: Comparing Doppler Profiling Radar and Surface  
689 Observations of Melting Level. *Journal of Hydrometeorology*, 9(2), 194–211.  
690 <https://doi.org/10.1175/2007jhm853.1>

691 Mann, M. E. (2004). On smoothing potentially non-stationary climate time series. *Geophysical*  
692 *Research Letters*, 31(January), 18–21. <https://doi.org/10.1029/2004GL019569>

693 Mazor, R. D., May, J. T., Sengupta, A., McCune, K. S., Bledsoe, B. P., & Stein, E. D. (2017). Tools  
694 for managing hydrologic alteration on a regional scale: Setting targets to protect stream health.  
695 *Freshwater Biology*, 786–803. <https://doi.org/10.1111/fwb.13062>

696 Mount, J. F. (1995). *California Rivers and Streams: The Conflict Between Fluvial Process and Land*  
697 *Use*. Berkeley: University of California Press.

698 Olden, J. D., & Poff, N. L. (2003). Redundancy and the choice of hydrologic indices for  
699 characterizing streamflow regimes. *River Research and Applications*, 19(2), 101–121.  
700 <https://doi.org/10.1002/rra.700>

701 Palshikar, G. (2009). Simple Algorithms for Peak Detection in Time- Series Simple Algorithms for  
702 Peak Detection in Time-Series. In *Proc. 1st Int. Conf. Advanced Data Analysis, Business*  
703 *Analytics and Intelligence*.

704 Pasternack, G. B., & Hinnov, L. A. (2003). Hydrometeorological controls on water level in a  
705 vegetated Chesapeake Bay tidal freshwater delta, 58, 367–387. [https://doi.org/10.1016/S0272-](https://doi.org/10.1016/S0272-7714(03)00106-9)  
706 [7714\(03\)00106-9](https://doi.org/10.1016/S0272-7714(03)00106-9)

707 Paul, S., & Hsu, H.-H. (2012). Comparative Study of Performance of CMIP3 GCMs in Simulating the  
708 East Asian Monsoon Variability. *Terrestrial, Atmospheric and Oceanic Sciences*, 23(4), 377–  
709 395. [https://doi.org/10.3319/TAO.2012.02.01.01\(A\)1](https://doi.org/10.3319/TAO.2012.02.01.01(A)1).

710 Poff, N. L., Allan, J. D., Bain, M. B., Karr, J. R., Prestegard, K. L., Richter, B. D., ... Stromberg, J.  
711 C. (1997). The natural flow regime. *Bioscience*, 47(11), 769–784. [https://doi.org/Doi](https://doi.org/10.2307/1313099)  
712 [10.2307/1313099](https://doi.org/10.2307/1313099)

713 Poff, N. L., & Ward, J. V. (1989). Implications of Streamflow Variability and Predictability for Lotic  
714 Community Structure: A Regional Analysis of Streamflow Patterns. *Canadian Journal of*  
715 *Fisheries and Aquatic Sciences*, 46(10), 1805–1818. <https://doi.org/10.1139/f89-228>

716 Poff, N. L., & Zimmerman, J. K. H. (2010). Ecological responses to altered flow regimes: a literature  
717 review to inform the science and management of environmental flows. *Freshwater Biology*,  
718 55(1), 194–205. <https://doi.org/10.1111/j.1365-2427.2009.02272.x>

719 Pollock, D. S. G. (1999). *A Handbook of Time-Series Analysis, Signal Processing and Dynamics*.  
720 London: The Academic Press. [https://doi.org/https://doi.org/10.1016/B978-0-12-560990-](https://doi.org/https://doi.org/10.1016/B978-0-12-560990-6.X5000-3)  
721 [6.X5000-3](https://doi.org/https://doi.org/10.1016/B978-0-12-560990-6.X5000-3)

722 Press, W. H., & Teukolsky, S. A. (1990). Savitzky-Golay Smoothing Filters. *Computers in Physics*,  
723 4(669). <https://doi.org/10.1063/1.4822961>

724 Ragozin, D. L. (1983). Error bounds for derivative estimates based on spline smoothing of exact or  
725 noisy data. *Journal of Approximation Theory*, 37(4), 335–355. [https://doi.org/10.1016/0021-](https://doi.org/10.1016/0021-9045(83)90042-4)  
726 [9045\(83\)90042-4](https://doi.org/10.1016/0021-9045(83)90042-4)

727 Richter, B. D., Baumgartner, J. V., Powell, J., & Braun, D. P. (1996). A Method for Assessing  
728 Hydrologic Alteration within Ecosystems. *Conservation Biology*, 10(4).

729 Rood, S. B., Samuelson, G. M., Braatne, J. H., Gourley, C. R., Hughes, F. M. R., Mahoney, J. M., &  
730 Hughes, F. (2005). Managing river flows to restore floodplain forests. *Frontiers in Ecology and*  
731 *the Environment*, 3(4), 193–201.

732 Sang, Y. F. (2013). A review on the applications of wavelet transform in hydrology time series  
733 analysis. *Atmospheric Research*, 122, 8–15. <https://doi.org/10.1016/j.atmosres.2012.11.003>

734 Sawaske, S. R., & Freyberg, D. L. (2014). An analysis of trends in baseflow recession and low-flows  
735 in rain-dominated coastal streams of the pacific coast. *Journal of Hydrology*, 519(PA), 599–  
736 610. <https://doi.org/10.1016/j.jhydrol.2014.07.046>

737 Schneider, R. (2011). *Survey of Peaks / Valleys identification in Time Series*.

738 Scholkmann, F., Boss, J., & Wolf, M. (2012). An Efficient Algorithm for Automatic Peak Detection in  
739 Noisy Periodic and Quasi-Periodic Signals. *Algorithms*, 5, 588–603.  
740 <https://doi.org/10.3390/a5040588>

741 Serreze, M. C., Clark, M. P., Armstrong, R. L., McGinnis, D. A., & Pulwarty, R. S. (1999).  
742 Characteristics of the western United States snowpack from snowpack telemetry (SNOTEL)  
743 data. *Water Resources Research*, 35(7), 2145–2160. <https://doi.org/10.1029/1999wr900090>

744 Smith, B, Schwartz, S, 2017. Automating Recession Curve Displacement Recharge  
745 Estimation. *Groundwater* 55 (1), 81–87. doi:10.1111/gwat.12439. In press.

746 Stewart, I. T. (2008). Changes in snowpack and snowmelt runoff for key mountain regions.  
747 *Hydrological Processes*, 23(1), 78–94. <https://doi.org/10.1002/hyp.7128>

748 Stewart, I. T., Ficklin, D. L., Carrillo, C. A., & McIntosh, R. (2015). 21st century increases in the  
749 likelihood of extreme hydrologic conditions for the mountainous basins of the Southwestern  
750 United States. *Journal of Hydrology*, 529, 340–353  
751 <https://doi.org/10.1016/j.jhydrol.2015.07.043>

752 Sultana, R., & Choi, M. (2018). Sensitivity of Streamflow Response in the Snow-Dominated Sierra  
753 Nevada Watershed Using Projected CMIP5 Data. *Journal of Hydrologic Engineering*, 23(8), 1–  
754 12. [https://doi.org/10.1061/\(ASCE\)HE.1943-5584.0001640](https://doi.org/10.1061/(ASCE)HE.1943-5584.0001640).

755 Thomas, B. F., Vogel, R. M., & Famiglietti, J. S. (2015). Objective hydrograph baseflow recession  
756 analysis. *Journal of Hydrology*, 525, 102–112. <https://doi.org/10.1016/j.jhydrol.2015.03.028>

757 Verveer, P. J. (2003). SciPy Reference Guide: Multi-dimensional image processing - “gaussian  
758 filter1d” and “gaussian filter.”

759 Wahba, G. (1978). Improper Priors , Spline Smoothing and the Problem of Guarding Against Model  
760 Errors in Regression. *Journal of the Royal Statistical Society. Series B (Methodological)*.,  
761 40(3), 364–372.

762 Yarnell, S. M., Viers, J. H., & Mount, J. F. (2010). Ecology and Management of the Spring Snowmelt  
763 Recession. *BioScience*, 60(2), 114–127. <https://doi.org/10.1525/bio.2010.60.2.6>

764 Yarnell, S. M., Petts, G. E., Schmidt, J. C., Whipple, A. A., Beller, E. E., Dahm, C. N., ... Viers, J. H.  
765 (2015). Functional Flows in Modified Riverscapes: Hydrographs, Habitats and Opportunities.  
766 *BioScience*, 65(10), 963–972. <https://doi.org/10.1093/biosci/biv102>

767 Yarnell, S. M., Stein, E. D., Webb, J. A., Grantham, T., Lusardi, R. A., Zimmerman, J., ... Sandoval-  
768 Solis, S. (2020). A functional flows approach to selecting ecologically relevant flow metrics for  
769 environmental flow applications. *River Research and Applications*, 36(2), 1–7.  
770 <https://doi.org/10.1002/rra.3575>

771 Zhang, H., Huang, Q., Zhang, Q., Gu, L., Chen, K., & Yu, Q. (2016). Changes in the long-term  
772 hydrological regimes and the impacts of human activities in the main. *Hydrological Sciences*  
773 *Journal*, 61(6), 1054–1068. <https://doi.org/10.1080/02626667.2015.1027708>

774 Zimmerman, J. K. H., Carlisle, D. M., May, J. T., Klausmeyer, K. R., Grantham, T. E., Brown, L. R.,  
775 & Howard, J. K. (2017). Patterns and magnitude of flow alteration in California , USA.  
776 *Freshwater Biology*, 859–873. <https://doi.org/10.1111/fwb.13058>

777

778